THE UNIVERSITY of EDINBURGH

Edinburgh Research Explorer

Changes to lipid droplet configuration in mCMV-infected fibroblasts: live cell imaging with simultaneous CARS and two-photon fluorescence microscopy

Citation for published version:
Wong, CSY, Robinson, I, Ochsenkuehn, MA, Arlt, J, Hossack, WJ & Crain, J 2011, 'Changes to lipid droplet configuration in mCMV-infected fibroblasts: live cell imaging with simultaneous CARS and two-photon fluorescence microscopy' Biomedical Optics Express, vol. 2, no. 9, pp. 2504-2516. DOI: 10.1364/BOE.2.002504

Digital Object Identifier (DOI):
10.1364/BOE.2.002504

Link:
Link to publication record in Edinburgh Research Explorer

Document Version:
Publisher's PDF, also known as Version of record

Published In:
Biomedical Optics Express

Publisher Rights Statement:
This paper was published in Biomedical Optics Express and is made available as an electronic reprint with the permission of OSA. The paper can be found at the following URL on the OSA website: http://dx.doi.org/10.1364/BOE.2.002504. Systematic or multiple reproduction or distribution to multiple locations via electronic or other means is prohibited and is subject to penalties under law.

General rights
Copyright for the publications made accessible via the Edinburgh Research Explorer is retained by the author(s) and / or other copyright owners and it is a condition of accessing these publications that users recognise and abide by the legal requirements associated with these rights.

Take down policy
The University of Edinburgh has made every reasonable effort to ensure that Edinburgh Research Explorer content complies with UK legislation. If you believe that the public display of this file breaches copyright please contact openaccess@ed.ac.uk providing details, and we will remove access to the work immediately and investigate your claim.

Download date: 05. Apr. 2019

Changes to lipid droplet configuration in mCMV-infected fibroblasts: live cell imaging with simultaneous CARS and two-photon fluorescence microscopy

Christine S. Y. Wong,[1,*] Iain Robinson,[1] Michael A. Ochsenkühn,[2] Jochen Arlt,[1] William J. Hossack,[1] and Jason Crain[1]

[1]*Collaborative Optical Spectroscopy Micromanipulation and Imaging Centre (COSMIC), School of Physics and Astronomy, The University of Edinburgh, Edinburgh, Mayfield Road, Edinburgh, EH9 3JZ, UK*
[2]*School of Chemistry, The University of Edinburgh, West Mains Road, Edinburgh, EH9 3JJ, UK*

**c.s.y.wong@ed.ac.uk*

Abstract: We have performed multimodal imaging of live fibroblast cells infected by murine cytomegalovirus (mCMV). The infection process was monitored by imaging the two-photon fluorescence signal from a GFP-expressing strain of mCMV, whilst changes to lipid droplet configuration were observed by CARS imaging. This allowed us to identify three visually distinct stages of infection. Quantitative analysis of lipid droplet number and size distributions were obtained from live cells, which showed significant perturbations across the different stages of infection. The CARS and two-photon images were acquired simultaneously and the experimental design allowed incorporation of an environmental control chamber to maintain cell viability. Photodamage to the live cell population was also assessed.

© 2011 Optical Society of America

OCIS codes: (180.0180) Microscopy; (170.3880) Medical and biological imaging; (170.1530) Cell analysis; (190.4380) Nonlinear optics, four-wave mixing; (170.2520) Fluorescence microscopy.

References and links

1. I. Robinson, M. A. Ochsenkühn, C. J. Campbell, G. Giraud, W. J. Hossack, J. Arlt, and J. Crain, "Intracellular imaging of host-pathogen interactions using combined CARS and two-photon fluorescence microscopies," J. Biophoton. **3**, 138–146 (2010).
2. J. Cheng, "Coherent anti-Stokes Raman scattering microscopy," Appl. Spectrosc. **61**, 197A–208A (2007).
3. C. L. Evans and X. S. Xie, "Coherent anti-Stokes Raman scattering microscopy: chemical imaging for biology and medicine," Annu. Rev. Anal. Chem. **1**, 883–909 (2008).
4. Y. Guo, K. R. Cordes, R.V. Farese, and T.C. Walther, "Lipid droplets at a glance," J. Cell Sci. **122**, 749–752 (2009).
5. D. M. Jones and J. McLauchlan, "Hepatitis C virus: assembly and release of virus particles," J. Biol. Chem. **285**, 22733–22739 (2010).
6. R. K. Lyn, D. C Kennedy, A. Stolow, A. Ridsdale, and J. P. Pezacki, "Dynamics of lipid droplets induced by the hepatitis C virus core protein," Biochem. Biophys. Res. Commun. **399**, 518–524 (2010).
7. E. Herker, C. Harris, C. Hernandez, A. Carpentier, K. Kaehlcke, A. R. Rosenberg, R. V. Farese, and M. Ott, "Efficient hepatitis C virus particle formation requires diacylglycerol acyltransferase-1," Nat. Med. **16**, 1295–1298 (2010).
8. R. Bartenschlager, F. Penn, V. Lohmann and P. Andre, "Assembly of infectious hepatitis C virus particles," Trends Microbiol. **19**, 95–103 (2010).

#147177 - $15.00 USD Received 9 May 2011; revised 5 Jun 2011; accepted 8 Jul 2011; published 2 Aug 2011

9. A. Angulo, P. Ghazal, and M. Messerle, "The major immediate-early gene *ie3* of mouse cytomegalovirus is essential for viral growth," J. Virol. **74**, 11129–11136 (2000).
10. N. E. Bishop, "Hepatitis A virus replication: an intermediate in the uncoating process," Intervirology **43**, 36–47 (2000).
11. G. Sluder, J. J. Nordberg, F. J. Miller, and E. H. Hinchcliffe, "A sealed preparation for long-term observations of cultured cells," in *Live Cell Imaging: A Laboratory Manual*, R. D. Goldman and D. L. Spector eds. (Cold Spring Harbor Laboratory Press, 2005), pp. 345–349.
12. D. J. Stevenson, D. J. Carnegie, B. Agate, F. Gunn-Moore, and K. Dholakia, "Long-term cell culture on a microscope stage: the carrel flask revisited." Microsc. Anal. **22**, 9–11 (2008).
13. M. E. Dailey, D. C. Focht, A. Khodjakov, C. L. Rieder, K. R. Spring, N. S. Claxton, S. G. Olenych, J. D. Griffin, and M. W. Davidson, "Maintaining live cells on the microscope stage," http://www.microscopyu.com/articles/livecellimaging/livecellmaintenance.html.
14. E. S. Mocarski, T. Shenk, and R. F. Pass, "Cytomegaloviruses," in *Fields Virology*, D. M. Knipe and P. M. Howley eds. (Lippincott Williams and Wilkins, 2006) pp. 2702–2772.
15. A. Yu, X. Ye, D. Ionascu, W. Cao, and P.M. Champion, "Two-colour pump-probe laser spectroscopy instrument with picosecond time-resolved electronic delay and extended scan range," Rev. Sci. Instrum. **76** 114301 (2005).
16. X. Nan, J. X. Cheng, and X. S. Xie, "Vibrational imaging of lipid droplets in live fibroblast cells with coherent anti-Stokes Raman scattering microscopy," J. Lipid. Res. **44**, 2202–2208 (2003).
17. W. Denk, D. W. Piston, and W. W. Webb, "Multi-photon molecular excitation in laser scanning microscopy," in *Handbook of Biological Confocal Microscopy* J. B. Pawley, (Springer, 2006) pp. 535–549.
18. J. Bewersdorf and S. W. Hell, "Picosecond pulsed two-photon imaging with repetition rates of 200 and 400 MHz," J. Microsc. **191**, 28–38 (1998).
19. M. A. Hayat, "Chemical fixation," in *Principles and Techniques of Electron Microscopy Biological Applications* (Cambridge University Press, 2000), pp. 43–44.
20. H. Fried and U. Kutay, "Nucleocytoplasmic transport: taking an inventory," Cell. Mol. Life Sci. **60**, 1659–1688 (2003).
21. W. Muranyi, J. Haas, M. Wagner, G. Krohne, and U. H. Koszinowski, "Cytomegalovirus recruitment of cellular kinases to dissolve the nuclear lamina," Science **297**, 854–857 (2002).
22. W. S. Rasband, "ImageJ," U. S. National Institutes of Health, http://imagej.nih.gov/ij/.

1. Introduction

The physical dimensions of viruses are smaller than the resolution limit of far field microscopy thereby precluding direct observation. As a result, many studies focus on examining the host–pathogen interactions which can be observed with far field microscopy. These studies generally involve labelling cells with fluorescent markers. However, labels can degrade into toxic photochemical reaction products and can also perturb the native biochemical pathways which operate between host and pathogen. This has restricted many previous investigations to working with fixed rather than living cells.

In this paper we demonstrate the application of far field microscopy to the study of host–pathogen interactions in unlabelled live cells. Specifically, we examine the correlation between cytomegalovirus infection and the behaviour of cellular lipid droplets by imaging live cells on a multimodal microscope platform which combines coherent anti-Stokes Raman scattering (CARS) and two-photon fluorescence (TPF). This work extends our previous study [1] which was based only on fixed cell samples.

The importance of label-free live cell imaging has led to the development of a variety of new methods for far field microscopy. Among them, CARS has emerged as the ideal technique for imaging cellular lipid droplets [2, 3]. The basic functions of lipid droplets as a store for energy reserves, hydrophobic compounds, and membrane building blocks have long been understood [4]. Recently, the more subtle and complex role played by these organelles has been revealed, including the discovery that lipid droplets are appropriated by the hepatitis C virus during the infection cycle [5–8]. CARS is clearly a valuable tool for the study of the link between lipids and viral replication. Used alone however, CARS is insufficient for identifying the infection state of cells, so we combine CARS with TPF to simultaneously image cellular lipid droplets whilst identifying and monitoring viral activity using a genetically modified

#147177 - $15.00 USD Received 9 May 2011; revised 5 Jun 2011; accepted 8 Jul 2011; published 2 Aug 2011
(C) 2011 OSA

murine cytomegalovirus (mCMV). The virus causes the host cell to express green fluorescent protein (GFP) upon infection.

The use of the modified virus allows the cellular expression of GFP to be utilised as a definitive marker of infection, to indicate that cellular translation of viral mRNA has begun. The modified genetic code persists in the DNA of viral progeny, therefore GFP expression continues for an extended time period after the initial infection. Furthermore, with this technique, it is possible to use the GFP expression to correlate observed cell changes with the overall timescale of the infection process. This imaging technique avoids the problems of toxicity, changes to cell function and fluorophore fading inherent to fluorescent labels.

In our previous study [1] we combined CARS and TPF imaging to compare fixed samples of healthy (uninfected) and infected mouse fibroblast cells. The main results were that the virus causes morphological changes to the cell, including expansion of the cell nucleus, and that an apparent rearrangement of lipid droplets occurs at some point during the infection process.

The aim of this study is to understand this dynamic process by relating the observed changes in lipid droplet configuration with the GFP expression, and hence the infection stage. A preliminary study of fixed cell samples is used to systematically identify the stages of viral infection by observing the quantity of GFP expression within the cell. We then image the lipid droplet behaviour in live cells during the infection process by using the fixed cell data as a reference to identify the stage of infection from the level of GFP expression.

2. Experimental Method

2.1. Sample Preparation

The method for sample preparation and infection with the genetically modified virus was described in detail in a previous paper [1]. Briefly, NIH/3T3 fibroblast cells with a passage number in the range 11–20 were cultured in Dulbecco's modified Eagle's medium (DMEM), with L-glutamine (200 mol/m^3), penicillin/streptomycin (10 000 units/ml) and 10 % calf serum. Standard growth conditions of 37 °C and a 5 % CO_2 environment were maintained during an incubation period of 12 hours. Cells were seeded onto glass-bottom Petri dishes (P35Gcol-1.0-14-C, MatTec). Infection with mCMV wildtype mutant C3X was carried out using a genetically modified version of the Smith strain [9] at a multiplicity of infection of 1, with the growth media containing 3 % calf serum in order to reduce cell growth.

2.2. Preliminary Study

A preliminary study was conducted with fixed cells, prepared as described above, with the exception that the cells were seeded onto glass coverslips and fixed using 1 % formaldehyde in phosphate buffered saline. By using a synchronized transfection method [10] a range of samples were fixed at known time points between 0 and 96 hours post transfection (hpt). The samples therefore consisted of a large number of cells fixed at the same time (hpt) in the infection cycle.

2.3. Live Cell Chamber

A portable cell chamber was built to provide a suitable environment for sustaining live cells on the microscope stage. The chamber was designed to attach directly onto the microscope, as shown in Fig. 1. Since the function of the chamber was to sustain a stable population of living cells, access for passaging or perfusion was not required. Therefore, the chamber was designed to be airtight, to maintain a 5 % CO_2 atmosphere, and to provide a controlled temperature of 37.0 °C [11]. The top window of the chamber was designed to touch the growth media in order to minimize signal loss due to refraction and to prevent the formation of condensation on the glass. We found that this set-up enabled live cells to survive on the microscope for at

#147177 - $15.00 USD Received 9 May 2011; revised 5 Jun 2011; accepted 8 Jul 2011; published 2 Aug 2011
(C) 2011 OSA

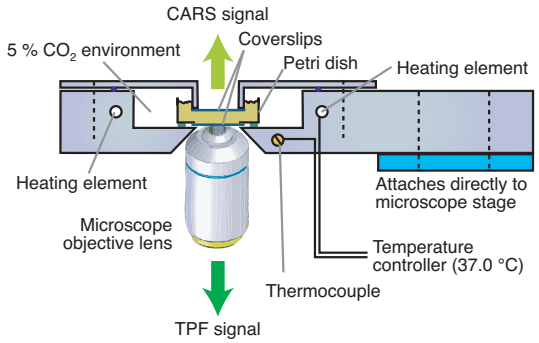

Fig. 1. Portable cell chamber for live cell imaging. A glass-bottom Petri dish containing the cell sample is sealed into the chamber in a 5 % CO_2 environment. The aluminium chamber body is fitted with heating elements and connected to a temperature controller which maintains a constant temperature of 37.0 °C. The chamber attaches directly to the stage of the (custom-built) microscope.

least 7 days. This was verified by observing a gradual growth in cell population from the initial 50–70 % to 100 % confluence over the period. A phenol-red indicator confirmed that neutral pH was maintained, suggesting that the CO_2 concentration remained constant inside the chamber [12, 13]. As cytomegalovirus completes its replication cycle after 72 hours at most [14], the longevity of cells in the chamber is more than sufficient for the process being investigated.

2.4. Imaging Instrumentation

A custom-built laser-scanning inverted CARS microscope setup [1], shown in Fig. 2, was used to record both CARS and TPF images simultaneously. The laser source was a pair of titanium-sapphire lasers (Mira 900, Coherent), which were mode-locked and synchronized via a phase-locked loop system [15] (Synchrolock, Coherent).

The 2845 cm^{-1} Raman vibration, which corresponds with the aliphatic C–H vibrations found in lipids [16], was targeted by tuning the pump laser wavelength to 714 nm and the Stokes laser to 896 nm. This generated a CARS signal at 593 nm, which was reflected out of laser beam path with a long wave-pass dichroic mirror (683dcxr, Chroma) and further filtered with a short wave-pass filter (680/SP-25, Semrock) and a narrow band-pass filter (600/14-25, Semrock). The forward CARS (F-CARS) signal was detected with a photomultiplier tube (PMT) (R3896, Hamamatsu).

The Stokes beam at 896 nm falls within the excitation band of GFP, allowing simultaneous TPF imaging with CARS. Unlike CARS, TPF is non-directionally scattered [17] and is most efficiently collected in the backward direction. A dichroic mirror behind the objective lens reflected the TPF signal out of the beam path. An identical PMT (R3896) was used to detect the signal. Two filters, a short wave-pass (680/SP-25, Semrock) and a broad band-pass (510/84-25, Semrock), were used to block the pump and Stokes laser wavelengths whilst transmitting most of the GFP emission spectrum. The band-pass filter also blocks the CARS signal at 593 nm. The picosecond pulse duration used in this set-up is ideal for CARS microscopy, but less so for TPF. Nonetheless, it is still capable of producing high-quality TPF images [18].

Image acquisition was achieved with a customized LabVIEW program, which controls the beam scanning mirrors and records the CARS and TPF PMT signals. The laser power at the sample was adjusted with neutral density filters (not shown in the figure). Bright field microscopy was used for all sample alignment and focusing in order to minimize the exposure of the sample to the laser beam.

#147177 - $15.00 USD Received 9 May 2011; revised 5 Jun 2011; accepted 8 Jul 2011; published 2 Aug 2011
(C) 2011 OSA

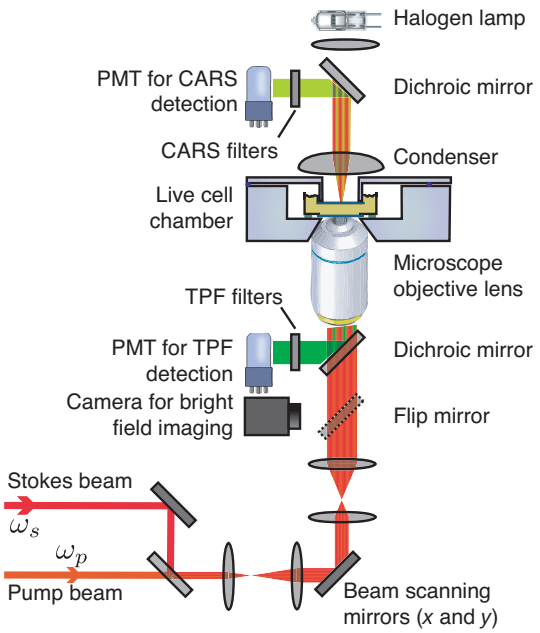

Fig. 2. Multimodal CARS and TPF microscopy system. The Stokes laser is tuned to 896 nm and the pump to 714 nm, to target a Raman shift of 2845 cm^{-1}. The two lasers are mode-locked and the pulses are synchronized. An *x*–*y* pair of galvanometer mirrors is used to scan the combined beams across the sample. The CARS signal is detected by a photomultiplier tube (PMT) in the forward direction (F-CARS) and TPF is detected, also by a PMT, in the backward direction. The set-up can also perform bright field imaging with a halogen lamp and camera.

3. Results and Discussion

3.1. Multimodal microscopy: simultaneous CARS and TPF

We used CARS to target the C–H Raman band at 2845 cm^{-1}. Bright spots were observed in the cytosol, which were identified as the resonant CARS signal from lipid droplets [16]. The cellular and nuclear membranes were also visible in CARS images due to the nonresonant background, revealing the cell morphology and the outline of the nucleus as a dark elliptical region.

Simultaneous and sequential CARS and TPF images are shown in Fig. 3. Sequential TPF images (Fig. 3(C)) were collected by scanning the Stokes laser beam only, the wavelength of which falls within the two-photon excitation band of GFP. It is evident that the TPF images generated simultaneously with CARS (Fig. 3(B)) are comparable to the images generated sequentially (Fig. 3(C)), with both TPF images revealing similar features. The bright high-contrast spots in the simultaneous image (Fig. 3(B)) could in principle arise from either CARS or GFP. To confirm that cross-channel leakage was not significant, pairs of images were taken with the phase of the pump and Stokes beams shifted by approximately 180° using the phase-locked loop system (Synchrolock). When the beams are out of phase, pump and Stokes pulses do not arrive at the sample simultaneously, so frequency mixing cannot occur and no CARS signal is generated. This test allows ready discrimination of the TPF signal from the CARS and confirmed that the filters prevented cross-channel leakage. The bright spots in TPF images recorded simultaneously with CARS (Fig. 3(B)) were therefore unambiguously identified as sites of GFP

#147177 - $15.00 USD Received 9 May 2011; revised 5 Jun 2011; accepted 8 Jul 2011; published 2 Aug 2011
(C) 2011 OSA

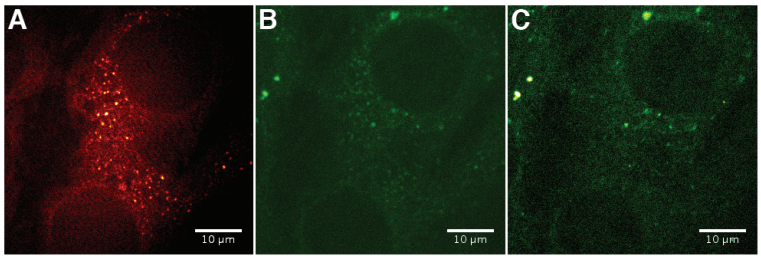

Fig. 3. Images of fibroblast cells infected with a genetically modified mCMV which causes cellular expression of GFP. The CARS image (A) shows the distribution of cellular lipid droplets. The TPF image (B), acquired simultaneously with the CARS, shows the sites of GFP, indicating that the cell is infected. A second TPF image (C) was recorded after the CARS image (sequentially) using only the Stokes laser beam; the pump beam was blocked.

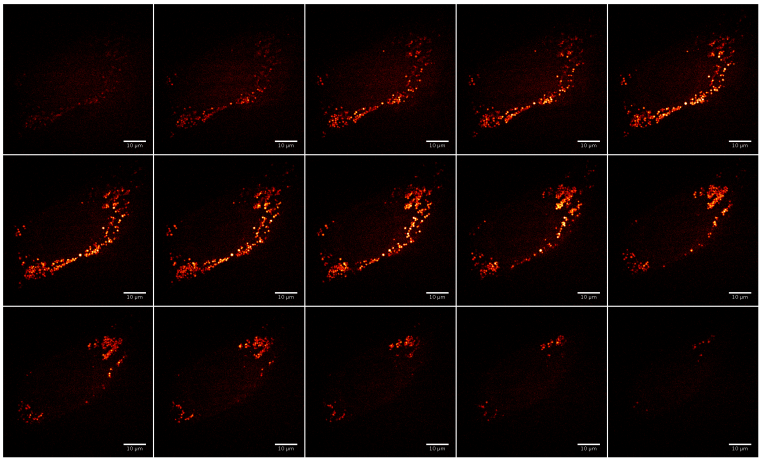

Fig. 4. A stack of CARS images through a single cell. Slices were taken at 0.25 μm increments in the z-direction. The laser power at the sample was approximately 35 mW. The bright spots visible in the images were identified as lipid droplets.

accumulation.

3.2. Cell Viability

The setup enabled acquisition of high-contrast CARS images using a reasonably low laser power of approximately 35 mW at the sample. Figure 4 shows a stack of images of a single live cell at increments of 0.25 μm, starting from the coverslip and scanning upwards in the z-direction. Bright field images were taken before (Fig. 5(A)) and after (Fig. 5(B)) recording the stack to assess possible photodamage. The image taken after recording the stack shows morphological changes to the cellular membrane, suggesting that some photodamage had occurred. Images of the same cell recorded two hours later, Fig. 6, revealed that the cell had become rounded and detached from the surface of the Petri dish. Nearby cells retained a normal appearance, indicating that the cell's death was due to photodamage.

The accumulated laser exposure experienced by a cell during stack acquisition is far greater than required for imaging a single slice. We tested cell viability against a range of laser powers in order to determine the optimum parameters for 2D imaging. We found that acquiring a 512×512 pixel image and integrating over 4 scans provided the optimum balance between

#147177 - $15.00 USD Received 9 May 2011; revised 5 Jun 2011; accepted 8 Jul 2011; published 2 Aug 2011
(C) 2011 OSA

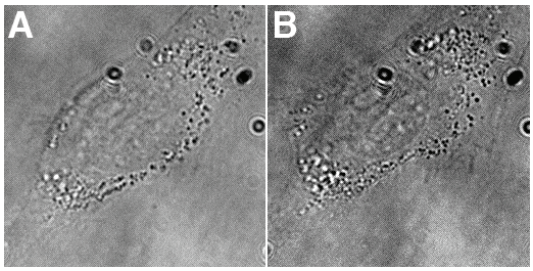

Fig. 5. Brightfield images recorded before (A) and after (B) the acquisition of the stack shown in Fig. 4. Visible photodamage is apparent after laser scanning.

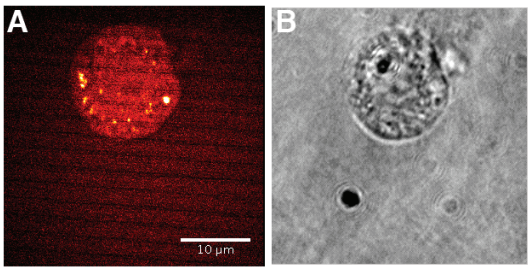

Fig. 6. CARS (A) and brightfield (B) images of the same cell shown in Fig. 4 and Fig. 5 recorded 2 hours after acquisition of the stack.

noise, image contrast and acquisition time. The minimum power achieved at these parameters was approximately 28 mW at the sample. Increasing the laser power increased the image contrast, but also increased the likelihood of photodamage.

Viability was tested with different cells over a range of laser powers in order to determine whether higher laser powers caused immediate damage to the cell morphology. It was found that powers up to 120 mW could be used without causing morphological changes in the cell on the timescale of the imaging. However the accumulated photodamage typically caused a delayed change in cell morphology after imaging. As a result, long time-course experiments, which involve imaging a single cell over many hours cannot be carried out at present. Instead, we are able to image many cells within the same live cell population over a time period of interest. This gives an overall view of the state of the cell population at the specific time point, and thus allows the change in overall cell population to be assessed over the time-course of infection.

3.3. Preliminary Study: Identification of Infection Stages

Samples of infected cells were fixed at 3 hour intervals and visually classified into three distinct groups: group 1, cells show low or nil concentrations of GFP, along with no significant changes to lipid droplet configurations compared to uninfected cells (0–9 hpt); group 2, cells show higher concentrations of GFP and significant changes to lipid droplet configuration (9–24 hpt); group 3, cells show major morphological changes and lipid droplet configuration changes, plus very high concentrations of GFP observed in the cells ($>$ 24 hpt). We refer to these groups respectively as the early, intermediate and late stages of infection.

All cell samples in the early infection stage (0–9 hpt) displayed similar features to those exhibited by the cell in Fig. 7. During this stage, CARS images showed both uniform size and spatial distributions of lipid droplets throughout the cytosol. TPF images had zero or limited

#147177 - $15.00 USD Received 9 May 2011; revised 5 Jun 2011; accepted 8 Jul 2011; published 2 Aug 2011
(C) 2011 OSA

contrast, indicating either no GFP, or the presence of a low concentration of GFP in the cytosol. There was no TPF signal from the nucleus, as GFP is expressed in the cytoplasm. The images also show areas of small accumulations of GFP in the cytosol, which could indicate the sites of GFP expression or suggest vesicle-mediated GFP transport.

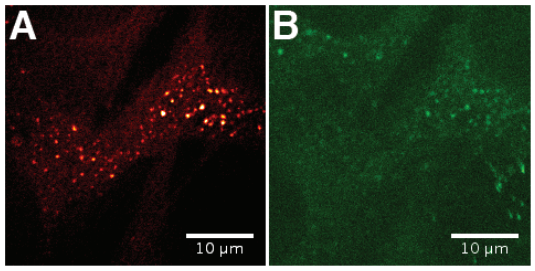

Fig. 7. CARS (A) and TPF (B) images of cells fixed at the early stage of infection. Lipid droplets of regular size are uniformly distributed in the cytosol. The low level of fluorescence provides limited contrast in the TPF image.

Cell samples infected for 9–24 hpt, the intermediate stage, typically exhibited the features shown in Fig. 8. The cells in this group displayed some lipid droplet clustering, where non-uniform spatial distributions of lipid droplets and some relatively large lipid droplets were identifiable. In addition, a general increase in cell nucleus area was evident. This is consistent with our earlier study [1], although in that investigation we were unable to associate nuclear expansion with a definite infection stage. The larger overall TPF signal indicated higher concentrations of GFP in the cytosol, thus confirming a progression of the infection.

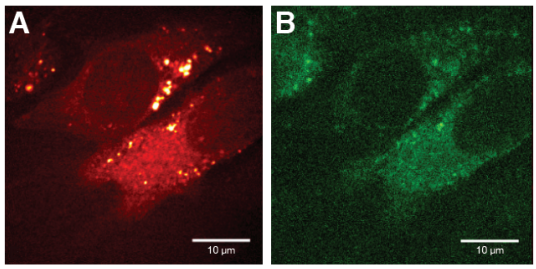

Fig. 8. CARS (A) and TPF (B) images of cells in the intermediate stage of infection. The distribution of lipid droplets is less uniform than in the early stage (Fig. 7) with the emergence of some clustering. The TPF image shows an increased amount of GFP expression.

Samples containing cells infected for $>$ 24 hpt, Fig. 9, we designated as the late stage of infection. Cells in this infection stage imaged using CARS show a dramatic reduction in the number of lipid droplets. The corresponding TPF images indicated high concentrations of GFP in both cytosol and nucleus, showing that GFP is imported into the cell nucleus at this late infection stage. Additionally, many images display fragmented cell nuclei, which suggests the cells are undergoing apoptosis.

Since GFP is expressed as a result of viral protein translation, we expect the fluorescence intensity to increase as the infection progresses. Figure 10 shows the measure of intensity of intracellular fluorescence per cell throughout the infection process. The graph shows a significant increase in fluorescence intensity as the infection progressed, where an average intensity of 17.3, 160.4 and 1025.9 (normalised units) was measured for each group of infected cells.

#147177 - $15.00 USD Received 9 May 2011; revised 5 Jun 2011; accepted 8 Jul 2011; published 2 Aug 2011
(C) 2011 OSA

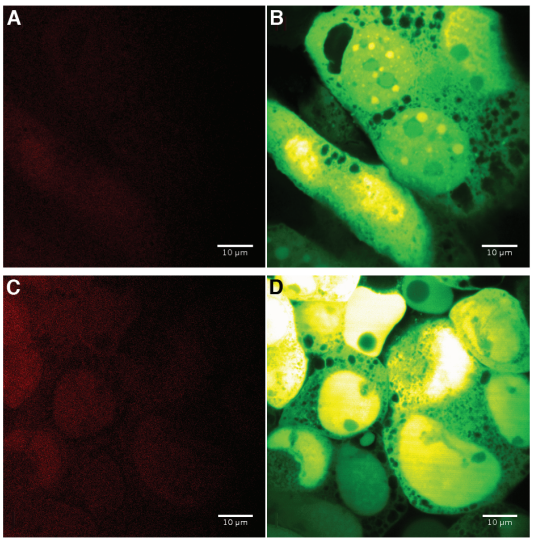

Fig. 9. CARS (A) and TPF (B) images of a sample of cells fixed in the late infection stage. (C) and (D) are CARS and TPF images of a different area of the same sample. The contrast in the two CARS images (A,C) is very limited due to the absence of lipid droplets. The TPF images (B,D) show a high level of GFP expression as well as fragmentation of cell nuclei suggesting apoptosis.

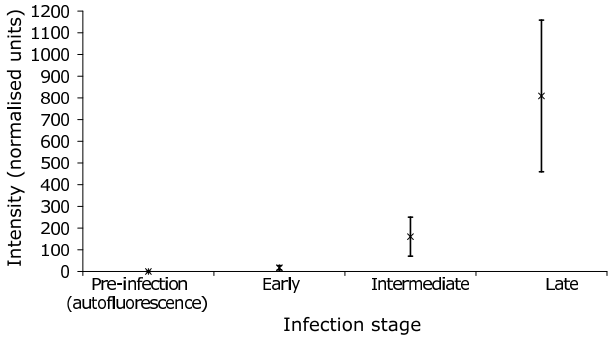

Fig. 10. Graph showing the average intensities for TPF images acquired pre-infection; and during the early, intermediate and late stages. Error bars indicate 1 standard deviation. To account for small changes in laser power between images the two-photon intensities have been normalized by dividing by the square of the power.

Pre-infection TPF images were also acquired where an average intensity of 0.09 was measured, indicating that there was no significant autofluorescence background in TPF images.

3.4. Imaging of Live Infected Cells

Although our preliminary study allowed us to group the infection process into three visually distinct stages, it is unsuitable for quantitative analysis of the observed changes in lipid droplet configuration because the formaldehyde fixing method causes rapid degradation of lipid droplets [19]. Therefore, the use of live cell samples is imperative for further analysis of lipid droplet characteristics during the infection process. Different cells in live samples had often progressed to different stages of the infection process, therefore within one image, each cell

#147177 - $15.00 USD Received 9 May 2011; revised 5 Jun 2011; accepted 8 Jul 2011; published 2 Aug 2011
(C) 2011 OSA

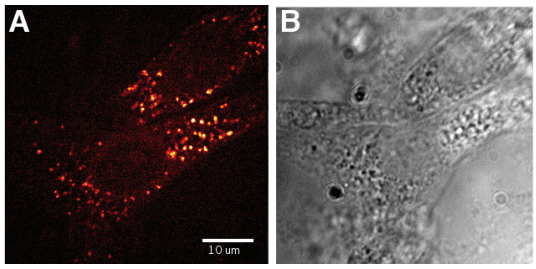

Fig. 11. CARS (A) and bright field (B) images of a group of live cells during the early stage of infection. The CARS image shows lipid droplets of regular size uniformly distributed throughout the cytosol. The pump and Stokes laser powers at the sample were approximately 25 mW and 30 mW respectively. The bright field image shows the cell outlines only.

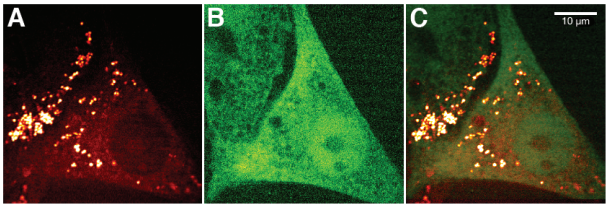

Fig. 12. CARS (A) and TPF (B) images of two cells in the intermediate stage of infection. The images are overlaid in (C). The pump and Stokes laser powers at the sample were approximately 28 mW and 32 mW respectively. The CARS image shows a non-uniform distribution of lipid droplets within the cytosol, with the appearance of clustering, specifically towards the neighbouring cell. The TPF image confirms that the cells are infected, and also shows that some GFP has been imported into the nucleus.

may be at a different stage of infection, as evident in Fig. 13(B). Using the data from the preliminary study we were able to assign the live cells to a definite stage (early, intermediate or late) of the infection process.

Cells in the early stage of infection provided a low overall intensity in TPF images. GFP expression is initiated by cellular translation of viral mRNA, therefore the initial appearance of GFP within the cell can be attributed to the onset of viral replication. CARS images of live cells acquired during the early infection stage, such as the image shown in Fig. 11, clearly show regularly-sized lipid droplets uniformly distributed throughout the cytosol, consistent with the preliminary study (Fig. 7).

CARS images acquired from cells in the intermediate stage of infection, such as the image shown in Fig. 12, showed non-uniform spatial distribution of lipid droplets throughout the cytosol. In addition, some relatively large lipid droplets were seen, suggesting a clustering effect. This behaviour is consistent with observations in the preliminary study (Fig. 8). Furthermore, some images of live cell infection, including Fig. 12, suggested that lipid droplets migrated towards neighbouring cells. Live cell TPF images revealed GFP in a number of cell nuclei. This feature was not observed in fixed cell images at the same infection stage, where GFP was only detected in the nucleus during the late stages of infection. These live cell images suggest that nuclear import of GFP occurs during the same infection stage as lipid droplet aggregation, indicating a possible link between the two processes. The import of GFP into the nucleus was an unexpected feature. Since GFP is synthesized in the cytosol, and nucleocytoplasmic transport is highly controlled [20], large molecules such as GFP must be actively transported in order to

#147177 - $15.00 USD Received 9 May 2011; revised 5 Jun 2011; accepted 8 Jul 2011; published 2 Aug 2011
(C) 2011 OSA

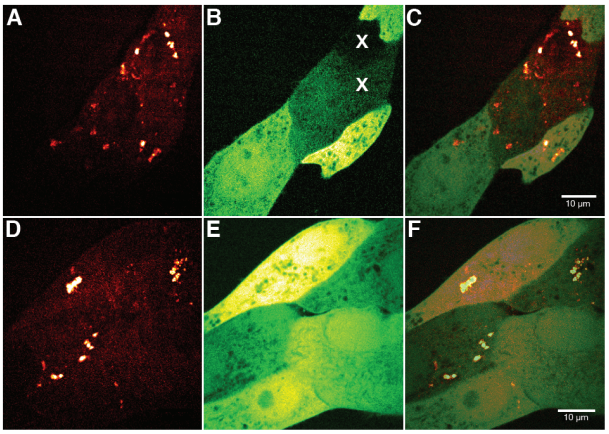

Fig. 13. CARS (A), TPF (B) and overlaid (C) images of a group of live cells in the late infection stage. (D–F) show a different group of cells. The pump and Stokes laser power at the sample was approximately 43 mW and 47 mW respectively. The CARS images (A,D) show a small number of lipid clusters. The high intensity in the corresponding TPF images (B,E) confirm the late stage of infection. Inhomogeneous infection is evident in image (B), where most cells are in the late infection stage with the exception of the two cells marked X which are in the intermediate stage, identified using fixed cell data as a reference.

enter the nucleus. This suggests that the behaviour may not be a cellular function initiated by the virus but rather a side-effect of infection caused by some mechanism occurring within the cell during the infection cycle [21].

CARS images of cells in the late stages of infection, Fig. 13, show a significant reduction in the number of lipid droplets. Where lipid droplets were still visible, much larger droplet sizes were typical. The high intensity in TPF images provided evidence of fragmented cells and apoptosis.

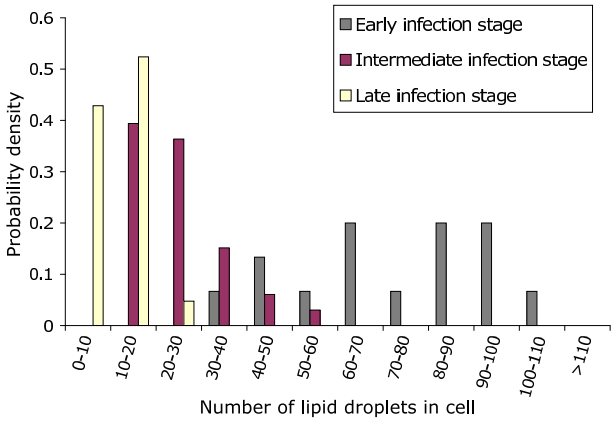

Fig. 14. Histogram showing the probability distribution of the number of lipid droplets in a cell for the early, intermediate and late infection stages. The separate counts for each infection stage group were binned and are plotted in the histogram. An empty bin for a particular infection stage indicates that there were no cells whose lipid droplet count was within the bin range.

#147177 - $15.00 USD Received 9 May 2011; revised 5 Jun 2011; accepted 8 Jul 2011; published 2 Aug 2011
(C) 2011 OSA

To confirm that the observed reduction in lipid droplet number is linked to the infection process, a sample of 69 cells was examined in more detail. The cells were first grouped into the three infection stages-early, intermediate and late-based on the level of GFP expression identified by the preliminary study. For each infection stage group, the number of lipid droplets per cell was counted. The histogram in Fig. 14 shows the probability that a cell has a given number of lipid droplets during the early, intermediate and late stages of infection. A clear decrease in lipid droplet number throughout the infection process is apparent. The mean number of lipid droplets are 63, 29 and 14, for the early, intermediate and late infection stages respectively, where the early infection probability distribution is between $37 \rightarrow 106$ lipid droplets, the intermediate infection probability distribution is between $12 \rightarrow 54$ lipid droplets, and the late infection probability distribution show that no cell contains more than 21 lipid droplets from the data set collected.

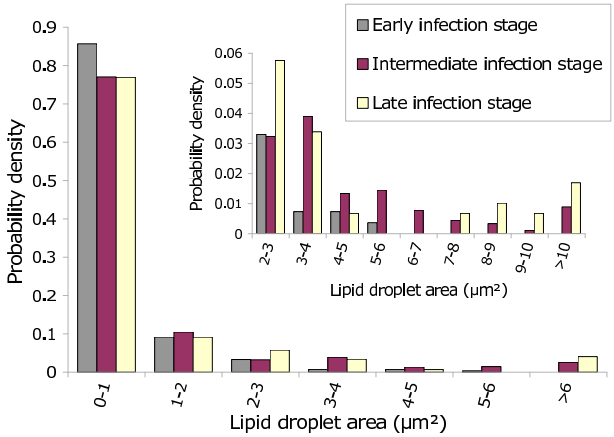

Fig. 15. Histogram showing the probability distribution of lipid droplet area for the early, intermediate and late infection stages. Inset: histogram (of the same data) showing the probability distribution of the lipid droplets with area greater than 2 μm^2.

In addition to a reduction in the number of lipid droplets, there appeared to be an increase in the size of the remaining droplets. In order to quantitatively determine the change in size due to clustering, the areas of lipid droplets were measured in a large sample of cells using ImageJ [22]. 545, 897 and 295 lipid droplet areas were measured for the early, intermediate and late infection stages respectively. A histogram showing the probability of measuring lipid droplets with a certain size during each infection stage is shown in Fig. 15. In the early infection stage, 86 % of the cells' lipid droplets were less than 1 μm^2 in size. This confirmed the observation in CARS images that lipid droplets were broadly similar in size during this infection stage. The graph also shows high probability of measuring lipid droplets with sizes less than 1 μm^2 for the intermediate and late infection stages, both 77 %. The difference between the lipid droplet sizes throughout the infection stages are most evident when looking at lipid droplets with area greater than 6 μm^2. In the intermediate infection stage, there was an increased probability of finding lipid droplets larger than 6 μm^2, with the probability further increasing in the late infection stage. No lipid droplets larger than 5.8 μm^2 were measured in cells in the early infection stage, showing that as the infection progresses, the probability of finding larger lipid droplets increases. This behaviour is highlighted by the inset in Fig. 15, where the histogram shows the probability distribution in more detail for the lipid droplets larger than 2 μm^2. These results confirm the observation of progressive lipid droplet clustering during infection.

#147177 - $15.00 USD Received 9 May 2011; revised 5 Jun 2011; accepted 8 Jul 2011; published 2 Aug 2011
(C) 2011 OSA

4. Conclusion

We have shown that a multimodal CARS and TPF microscope system allows the observation and measurement of changes in live fibroblast cells that occur during infection by cytomegalovirus. Imaging with TPF allowed us to identify three distinct stages of the infection process; early, intermediate and late infection stage, whilst simultaneous CARS imaging was used to observe the changes in cell morphology, and to quantify the perturbations to cellular lipid droplets, enabling us to correlate these findings against the defined infection stages. This enabled us to identify several persistent features of cytomegalovirus infection including a change in cell morphology, a decrease in the number of cellular lipid droplets and an overall increase in the size of the remaining droplets, thus suggesting a clustering of lipid droplets. The increase in the size was significant, with some lipid droplets of area greater than 6 μm^2 emerging in the later stages of infection. The biological significance of these observed processes requires further investigation.

Acknowledgments

We appreciate the provision of C3X-GFP virus from Mathieu Blanc of the Division of Pathway Medicine, University of Edinburgh.

#147177 - $15.00 USD Received 9 May 2011; revised 5 Jun 2011; accepted 8 Jul 2011; published 2 Aug 2011
(C) 2011 OSA